Polymer Chemistry

ROYAL SOCIETY OF CHEMISTRY

COMMUNICATION

View Article Online
View Journal | View Issue

Cite this: *Polym. Chem.*, 2022, **13**, 4366

Received 29th April 2022,
Accepted 11th July 2022

DOI: 10.1039/d2py00557c

rsc.li/polymers

Tailoring the luminescence of FRET systems built using supramolecular polymeric nanotubes†

Qiao Song, *[a,b] Jingyu Zhang,[a] Xinxin Yu,[a] Zihe Cheng,[b] Jie Yang, [b,c] Stephen C. L. Hall[b] and Sébastien Perrier *[b,d,e]

Supramolecular polymeric nanotubes self-assembled from cyclic peptide–polymer conjugates are employed as general scaffolds to fabricate supramolecular FRET systems. The monomer-to-excimer emission ratio of the FRET donor, PYR–CP–PEG, can be simply and reversibly tuned by the introduction of a spacer in the supramolecular structure, thus endowing the luminescent FRET systems with tailorable and responsive properties.

Introduction

Fluorescent materials with tuneable luminescence have attracted an increasing amount of attention in the fields of visual displays, illumination, bioimaging, and ion/molecular sensing.[1–8] Conventional approaches for controlling the emission of fluorescent molecules mainly involve covalent modification. Over the past few decades, a large variety of organic dyes have been developed with tailored photophysical properties.[9,10] Moreover, the innovation of organic molecular luminescence mechanisms, including intramolecular charge transfer (ICT),[11,12] twisted ICT (TICT),[13,14] Förster resonance energy transfer (FRET),[15] excited-state intramolecular proton transfer (ESIPT),[16] aggregation-induced emission (AIE),[17,18] and vibration-induced emission (VIE),[19,20] further advances the knowledge in the design of luminescent molecules. Supramolecular systems are spontaneously assembled structures constructed using relatively simple molecular building blocks through noncovalent interactions, including hydrogen bonding, host–guest interactions, π–π stacking, metal coordination, hydrophobic forces, and electrostatic interactions.[21–24] Different from their covalent counterparts, supramolecular chemistry focuses on reversible, dynamic, and responsive properties. As many of the organic molecular luminescence mechanisms are related to the molecular arrangement of dyes, supramolecular chemistry offers a complementary way of facilely and reversibly tuning the photophysical properties of fluorophores.[25–34]

FRET describes a photophysical process between two fluorophores in which energy is transferred from an excited donor to a proximal ground-state acceptor through non-radiative dipole–dipole coupling. Supramolecular FRET systems have found various applications, including fluorescence sensing, light harvesting, fluorescence imaging, intra- and intermolecular interaction determination, nanoscale structural and configurational analysis, and molecular dynamics studies.[35–37] Due to the strong dependence of the energy transfer efficiency on the donor–acceptor distance, accurately positioning multiple components into a highly organised assembled system is essential for the construction of fluorescent materials with tuneable luminescence properties. A wide range of supramolecular scaffolds, including micelles, vesicles, fibrils, supramolecular polymers, gels, and bio-inspired structures, have been used to construct supramolecular FRET systems, generating supramolecular luminescent materials with tuneable and dynamic properties.[38–41]

Self-assembling cyclic peptide–polymer conjugates are capable of stacking into supramolecular polymeric nanotubes in solutions with a well-defined core–shell structure.[42–46] The cyclic peptide constitutes the core driven by multiple hydrogen bonds, with the solvated polymer chains wrapped as the shell. The highly ordered supramolecular polymeric nanotubes have been employed as scaffolds to molecularly arrange functional moieties such as drugs, π-conjugated chromophores, proteins, and nanoparticles.[47–52] More recently, we built a supramolecular system with a two-step sequential FRET process by molecularly aligning three different chromophores along the nano-

[a]*Shenzhen Grubbs Institute, Southern University of Science and Technology, Shenzhen 518055, China. E-mail: songq@sustech.edu.cn*
[b]*Department of Chemistry, University of Warwick, Coventry CV4 7AL, UK. E-mail: s.perrier@warwick.ac.uk*
[c]*College of Science, Nanjing Forestry University, Nanjing 210037, China*
[d]*Warwick Medical School, University of Warwick, Coventry CV4 7AL, UK*
[e]*Faculty of Pharmacy and Pharmaceutical Sciences, Monash University, Parkville, VIC 3052, Australia*

† Electronic supplementary information (ESI) available. See DOI: https://doi.org/10.1039/d2py00557c

tubes, which showed great potential in artificial light-harvesting systems and highly emissive organic materials.[53] Considering its powerful capability of aligning chromophores and the resulted high energy transfer efficiency, we believe that the supramolecular polymeric nanotube could be employed as a general scaffold to fabricate supramolecular FRET systems with tailorable luminescence.

Herein, as shown in Scheme 1a, a fluorophore–cyclic peptide–polymer conjugate, PYR–CP–PEG, is chosen as the FRET donor due to its unique emission behaviour. The formation of the self-assembled polymeric nanotubes driven by multiple hydrogen bonds between the cyclic peptides leads to the stacking of pyrene moieties. As a result, a broader emission band belonging to the pyrene excimer appears accompanied by the conventional pyrene monomeric emission, thus effectively extending the emission of PYR–CP–PEG in water to a wide range between 350 nm and 650 nm.[54,55] This greatly expands the range of fluorophores as FRET acceptors to construct supramolecular FRET systems. Three fluorophore–cyclic peptide–polymer conjugates with distinctive fluorescence colours, NTI–CP–PEG, Cy3–CP–PEG, and Cy5–CP–PEG, are selected as FRET acceptors, generating three supramolecular FRET systems built using the supramolecular polymeric nanotubes. All the three systems showed high energy transfer efficiency, permitting a wide tuning range of fluorescence colours. Moreover, by the introduction of a spacer, Oct–CP–PEG in the stacked structures, the monomer-to-excimer emission ratio could be facilely and reversibly tuned (Scheme 1b). Owing to the distinct energy transfer capability between the pyrene monomer and excimer to energy acceptors, the overall energy transfer efficiency could be effectively altered. This offers a unique supramolecular strategy to tailor the luminescence of the supramolecular peptide nanotubes. Last but not least, by replacing Oct–CP–PEG with a pH-responsive conjugate, we were able to show that the energy transfer efficiency and fluorescence colour of the supramolecular FRET systems could be reversibly controlled by variation in pH.

Results and discussion

The energy transfer process between PYR–CP–PEG as the FRET donor and NTI–CP–PEG, Cy3–CP–PEG, or Cy5–CP–PEG as the FRET acceptor, respectively, was studied. As shown in Fig. 1a, despite the disparate absorption spectra of NTI–CP–PEG, Cy3–CP–PEG, and Cy5–CP–PEG peaked at 450 nm, 552 nm, and 650 nm, they all overlap with the emission spectrum of PYR–CP–PEG to some extent without exception. As a result, FRET occurred when co-assembling NTI–CP–PEG, Cy3–CP–PEG, or Cy5–CP–PEG with PYR–CP–PEG to form supramolecular polymeric nanotubes in water. The emission of PYR–CP–PEG kept decreasing when increasing the ratio of NTI–CP–PEG, Cy3–CP–PEG, or Cy5–CP–PEG, while a new emission band appeared at the same time, which could be ascribed to the emission of the corresponding acceptor fluorophore (Fig. 1b–d). The energy transfer process could be confirmed by time-resolved fluorescence experiments. As shown in Fig. S5–S7,† the fluorescence decay of PYR–CP–PEG was significantly faster in the presence of NTI–CP–PEG, Cy3–CP–PEG, or Cy5–CP–PEG (Table S1 and Fig. S8†).

As mentioned above, the donor emission is contributed by both the PYR monomer and excimer. The energy transfer efficiency (Φ_{ET}) from the PYR monomer or the excimer to NTI, Cy3, or Cy5 was then calculated. Taking PYR–CP–PEG/Cy3–CP–PEG as an example, as shown in Fig. S10,† each emission spectrum was convoluted into 3 emission bands from the PYR monomer, PYR excimer, and Cy3. This allows the accurate calculation of Φ_{ET} values, as indicated in Fig. S12.† With the increase of Cy3–CP–PEG ratio, both Φ_{ET} from the PYR monomer to Cy3 ($\Phi_{ET,\ Mon-Cy3}$) and Φ_{ET} from the PYR excimer to Cy3 ($\Phi_{ET,\ Exc-Cy3}$) increased. However, since the overlap between the PYR monomer emission spectrum and Cy3–CP–PEG absorption spectrum is significantly smaller than that between the PYR excimer emission spectrum and the Cy3–CP–PEG absorption spectrum, $\Phi_{ET,\ Mon-Cy3}$ is much lower than $\Phi_{ET,\ Exc-Cy3}$. For example, at a PYR–CP–PEG/Cy3–CP–PEG ratio

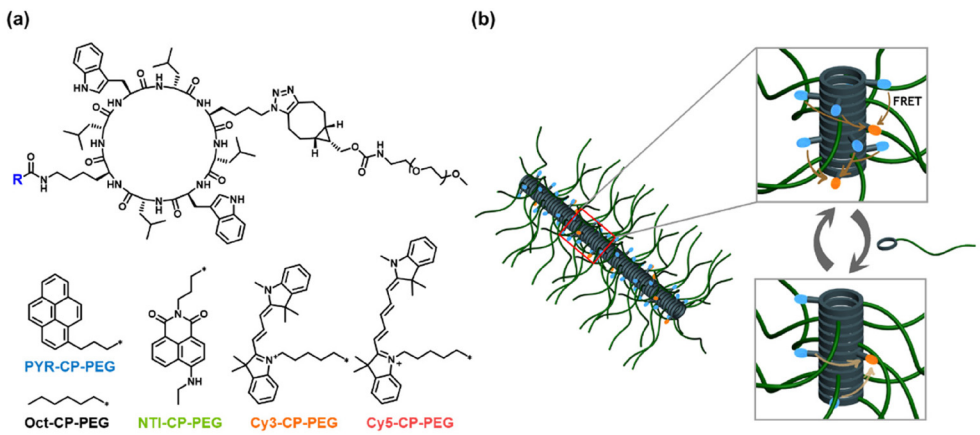

Scheme 1 FRET systems built using supramolecular polymeric nanotubes with tailorable luminescence: (a) chemical structures of the fluorophore–cyclic peptide–polymer conjugates and the spacer; (b) cartoon illustration of tailoring the luminescence of FRET systems with the supramolecular spacer.

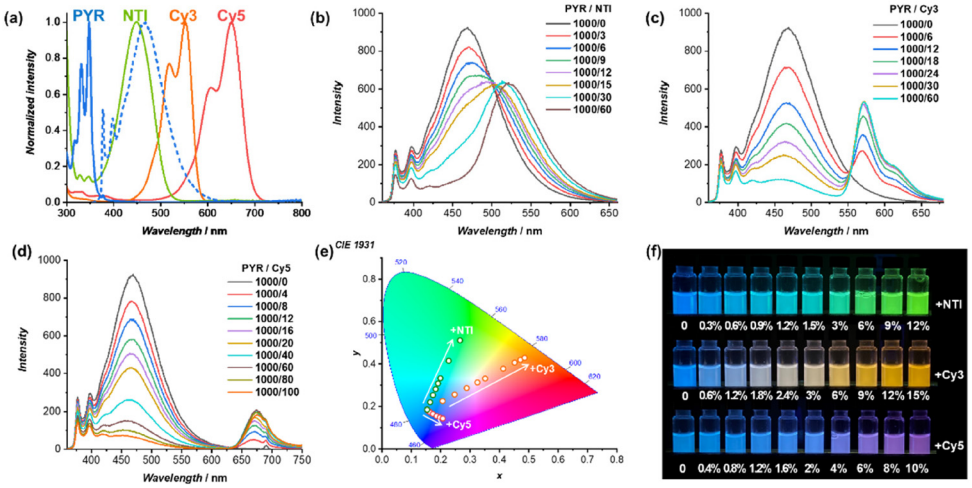

Fig. 1 (a) Normalized absorption spectra (solid curves) of PYR–CP–PEG (blue trace), NTI–CP–PEG (green trace), Cy3–CP–PEG (orange trace), and Cy5–CP–PEG (red trace), and the normalized fluorescence spectrum of PYR–CP–PEG (dashed curve, blue trace); (b) fluorescence spectra of PYR–CP–PEG with the addition of NTI–CP–PEG; (c) fluorescence spectra of PYR–CP–PEG with the addition of Cy3–CP–PEG; (d) fluorescence spectra of PYR–CP–PEG with the addition of Cy5–CP–PEG; (e) CIE 1931 diagram showing the CIE coordinates of fluorescence emission colours at different PYR–CP–PEG/NTI–CP–PEG, PYR–CP–PEG/Cy3–CP–PEG, and PYR–CP–PEG/Cy5–CP–PEG molar ratios; (f) photograph showing fluorescence emissions at different PYR–CP–PEG/NTI–CP–PEG, PYR–CP–PEG/Cy3–CP–PEG, and PYR–CP–PEG/Cy5–CP–PEG ratios, under a 365 nm UV lamp.

of 100/6, $\Phi_{ET,\ Exc-Cy3}$ is 89.1%, while $\Phi_{ET,\ Mon-Cy3}$ is only 30.2%. Similar trends could be observed for PYR–CP–PEG/NTI–CP–PEG and PYR–CP–PEG/Cy5–CP–PEG (Fig. S9, S11 and S12†). For all cases, the overall energy transfer efficiency ($\Phi_{ET,\ total}$) could reach 90% at relatively low donor/acceptor ratios, suggesting efficient FRET processes within the supramolecular polymeric nanotubes.

The efficient FRET process allows effective tailoring of the luminescence colour of the supramolecular polymeric nanotubes. As indicated in Fig. 1e and f, a series of fluorescence colours could be obtained in a wide range. Specifically, by increasing the ratio of NTI–CP–PEG to PYR–CP–PEG, the fluorescence colour could be tuned from blue to green; by increasing the ratio of Cy3–CP–PEG to PYR–CP–PEG, the fluorescence colour could be tuned from blue *via* white and finally to orange; by increasing the ratio of Cy5–CP–PEG to PYR–CP–PEG, the fluorescence colour could be tuned from blue to pink.

The monomer-to-excimer emission ratio of PYR could be tuned noncovalently by adjusting the stacking of pyrene moieties in the self-assembled polymeric nanotubes. To this end, a non-emissive conjugate, Oct–CP–PEG, was introduced as a supramolecular spacer to co-assemble with PYR–CP–PEG. The average distance between PYR moieties increased in the co-assemblies of PYR–CP–PEG/Oct–CP–PEG, thus causing a decrease in PYR excimer emission (Fig. 2a). As shown in Fig. 2b, with the increase of Oct–CP–PEG/PYR–CP–PEG ratio, a continuous decrease of the PYR excimer emission band peaked at 470 nm was observed, along with the simultaneous increase of PYR monomer emission. The increase in the average distance between PYR moieties was further confirmed by UV/vis spectroscopy. The absorption of the PYR moiety

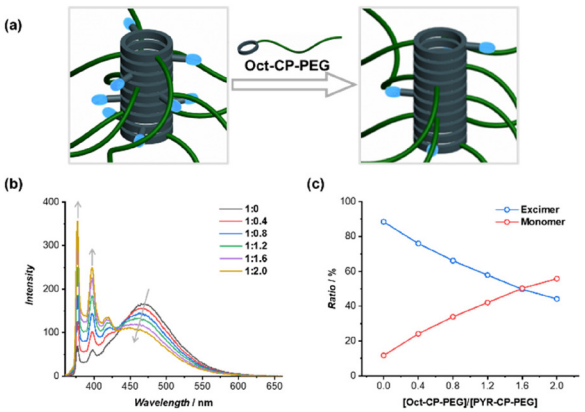

Fig. 2 (a) Schematic illustration showing the co-assembly of PYR–CP–PEG and Oct–CP–PEG; (b) fluorescence spectra of PYR–CP–PEG/Oct–CP–PEG at different molar ratios; (c) evolution of the ratio of PYR monomer and excimer emission at the Oct–CP–PEG/PYR–CP–PEG molar ratio.

increased gradually with a slight hypsochromic shift when increasing the ratio of Oct–CP–PEG/PYR–CP–PEG (Fig. S13†). The monomer-to-excimer emission ratio of PYR was then quantified by convoluting each emission spectrum into peaks of PYR monomer emission and PYR excimer emission (Fig. S14†). Fig. 2c shows the change of PYR monomer-to-excimer emission ratios at different Oct–CP–PEG/PYR–CP–PEG molar ratios. Initially, PYR–CP–PEG emission is composed of a large majority of excimer (88.4%) and a small portion of monomer (11.6%). With the increase of Oct–CP–PEG/PYR–CP–PEG molar ratio from 0/1 to 2/1, the ratio of the excimer gradually decreased to 44.2%, while that of the monomer increased

to 55.8%. Therefore, by co-assembling PYR–CP–PEG with Oct–CP–PEG as the spacer, the monomer-to-excimer emission ratio of PYR could be rationally tuned over a large range.

The distinct emission spectra of the PYR monomer and excimer lead to different energy transfer capabilities to energy acceptors. Hence, it is anticipated that the excimer-to-monomer emission transition of PYR will lead to a gradual decrease in the overall energy transfer efficiency. In this regard, Oct–CP–PEG was introduced into the FRET systems composed of PYR–CP–PEG as the energy donor and NTI–CP–PEG, Cy3–CP–PEG, or Cy5–CP–PEG as the energy acceptor. As shown in Fig. 3a, the addition of Oct–CP–PEG to the FRET system of PYR–CP–PEG/Cy3–CP–PEG = 100/6 resulted in a continuous decrease of Cy3 emission, accompanied by a dramatic increase of both PYR monomer and excimer emission. By convoluting the spectra into emission bands ascribed to the PYR monomer, PYR excimer, and Cy3, Φ_{ET} values including $\Phi_{ET,\ Mon-Cy3}$, $\Phi_{ET,\ Exc-Cy3}$, and $\Phi_{ET,\ total}$ were calculated (Fig. S17†). On one hand, the distance between PYR–CP–PEG and Cy3–CP–PEG increased when co-assembled with Oct–CP–PEG, which consequently caused the decrease of both $\Phi_{ET,\ Mon-Cy3}$ and $\Phi_{ET,\ Exc-Cy3}$ (Fig. 3b). On the other hand, the PYR monomer-to-excimer ratio increases with the increase in Oct–CP–PEG/PYR–CP–PEG molar ratio. The combination of both leads to a greater variation of $\Phi_{ET,\ total}$, decreasing from 83.7% to as low as 36.1%. As a result, the addition of Oct–CP–PEG enables reverse tuning of the fluorescence colour from orange *via* white to blue (Fig. 3c). Similar phenomena were observed for PYR–CP–PEG/NTI–CP–PEG and PYR–CP–PEG/Cy5–CP–PEG when adding Oct–CP–PEG (Fig. S15–S19†). It should be noted that the capability of tuning the PYR monomer and excimer emission ratio by the incorporation of a spacer is unique to this system, which allows a more effective tuning of Φ_{ET}, and hence a greater range of luminescence colours.

The dynamic nature of non-covalent interactions makes it facile to introduce stimuli-responsive features into the supramolecular FRET systems. As a proof of concept, we demonstrate here the capability of reversibly tuning the energy transfer efficiency and fluorescence colour by adjusting the pH. To this end, a pH-responsive conjugate was designed bearing two glutamic acid moieties on the cyclic peptide, namely Hep–CP–PEG (Fig. 4a). Under alkaline conditions, the electrostatic repulsion between the cyclic peptides originated from the deprotonated carboxyl groups will result in the disassembly of the polymeric nanotubes. Acidifying the solution will neutralize the cyclic peptide and lead to the re-assembly of the nanotubes. Therefore, we hypothesized that replacing Oct–CP–PEG with Hep–CP–PEG might not only allow the tuning of the energy transfer efficiency and fluorescence colour similar to Oct–CP–PEG but also allow the control of both by pH.

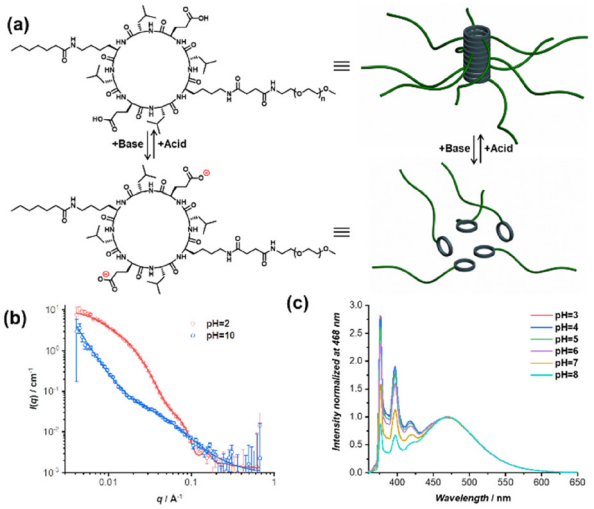

Fig. 4 (a) Schematic illustration showing the pH-responsiveness of Hep–CP–PEG; (b) SANS scattering data and fitting of Hep–CP–PEG at pH = 2 and pH = 10; (c) fluorescence spectra of PYR–CP–PEG/Hep–CP–PEG = 1/4 at different pH.

The pH-responsive properties of Hep–CP–PEG were demonstrated by ^{1}H NMR spectroscopy and small angle neutron scattering (SANS). As shown in the ^{1}H NMR spectra (Fig. S20†), at acidic pH, only proton resonances belonging to PEG were clearly observed, while those derived from the cyclic peptide (core) were almost invisible because of its low mobility within the polymeric nanotube. However, after adjusting the pH to basic, all peaks ascribed to the cyclic peptide became clear and sharp, implying the disassembly of the polymeric nanotubes. SANS provides more detailed information regarding the change of morphology when altering pH. As shown in Fig. 4b,

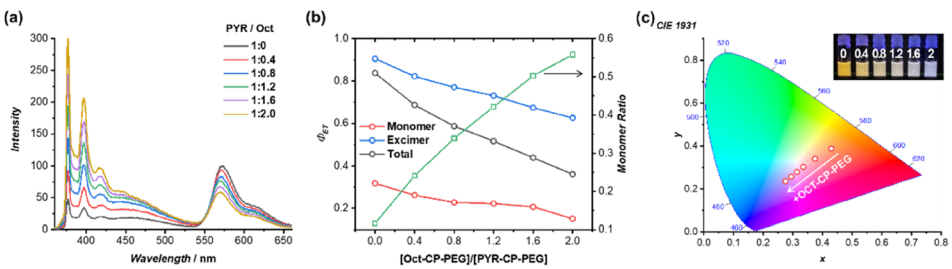

Fig. 3 Fluorescence spectra of PYR–CP–PEG/3%NTI–CP–PEG with the addition of different molar ratios of Oct–CP–PEG; (b) Φ_{ET} and PYR monomer ratios at different Oct–CP–PEG/PYR–CP–PEG molar ratios; (c) CIE 1931 diagram showing the CIE coordinates of (a) (insert: photograph showing fluorescence emissions of (a) under a 365 nm UV lamp).

at pH = 2, the SANS data were fitted using a cylindrical polymer micelle model, which agrees well with the proposed polymeric nanotubular structure (Table S2†); while at pH = 10, the data were fitted using a Gaussian coil model, suggesting the disassembly of the polymeric nanotubes (Table S3†).

The ability of tuning the PYR monomer-to-excimer ratio by Hep–CP–PEG was then investigated. As shown in Fig. S21,† with the increase of Hep–CP–PEG/PYR–CP–PEG molar ratio in an acidic environment, an increase of monomer-to-excimer ratio was observed, implying that Hep–CP–PEG could function similarly to Oct–CP–PEG. More importantly, the monomer-to-excimer ratio is sensitive to pH. At a fixed molar ratio of Hep–CP–PEG/PYR–CP–PEG = 4/1, the increase in pH led to an increase in monomer-to-excimer ratio (Fig. 4c and Fig. S22†). At pH = 3, the emission is composed of 61.8% excimer and 38.2% monomer; while at pH = 8, the excimer emission ratio increased to 83.7% with only 16.3% monomer remaining. This could be attributed to the pH-responsive property of Hep–CP–PEG. As the pH increases, an increased number of carboxyl groups on the cyclic peptides are deprotonated, which subsequently leads to a weakening co-assembly with PYR–CP–PEG.

Lastly, the pH-responsive properties of the supramolecular FRET systems in the presence of Hep–CP–PEG were studied. Fig. 5a shows the fluorescence spectra of PYR–CP–PEG/Cy3–CP–PEG/Hep–CP–PEG = 1/0.06/4 at different pH values. A clear decrease in PYR emission was observed when increasing pH. By comparing the emission spectra with the ones in the absence of Cy3–CP–PEG, Φ_{ET} values at different pH values were calculated (Fig. S23†). Both $\Phi_{ET,\ Mon-Cy3}$ and $\Phi_{ET,\ Exc-Cy3}$ increased with the increase of pH. Consequently, a greater increase of $\Phi_{ET,\ total}$ from 45.0% to 74.4% was achieved by increasing the pH from 3 to 8. In this way, the fluorescence colour could be adjusted from orange *via* white to light blue simply by decreasing the pH from 8 to 3 (Fig. 5b). This strategy is applicable to other FRET systems, including PYR–CP–PEG/NTI–CP–PEG and PYR–CP–PEG/Cy5–CP–PEG. As can be seen in Fig. 5c, distinct fluorescence colours were obtained at different pH values (Fig. S24†).

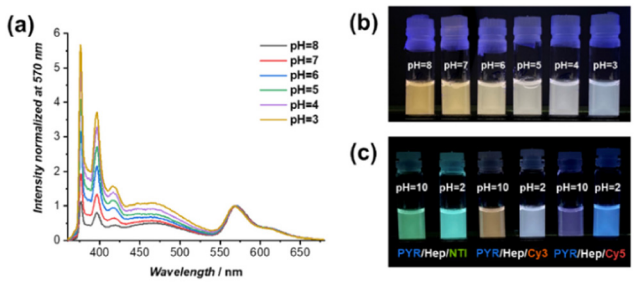

Fig. 5 (a) Fluorescence spectra of PYR–CP–PEG/Cy3–CP–PEG/Hep–CP–PEG = 1/0.06/4 at different pH; (b) photograph showing fluorescence emissions of PYR–CP–PEG/Cy3–CP–PEG/Hep–CP–PEG at different pH, under a 365 nm UV lamp; (c) photograph showing fluorescence emissions of PYR–CP–PEG/NTI–CP–PEG/Hep–CP–PEG, PYR–CP–PEG/Cy3–CP–PEG/Hep–CP–PEG, and PYR–CP–PEG/Cy5–CP–PEG/Hep–CP–PEG at pH = 2 and pH = 10, under a 365 nm UV lamp.

Conclusions

To conclude, we have successfully developed supramolecular FRET systems with tailorable luminescence based on supramolecular polymeric nanotubes. The unique excimer emission of the energy donor, PYR–CP–PEG, enables a wide range of fluorophores as FRET acceptors. Therefore, different supramolecular FRET systems with high energy transfer efficiency were constructed, showing tuneable luminescence colours, including blue, green, orange, and pink. More importantly, the excimer-to-monomer emission transition of PYR–CP–PEG induced by the incorporation of a supramolecular spacer led to a gradual decrease in the degree of spectral overlap between donor emission and acceptor absorption, offering a supramolecular strategy to tailor the luminescence of the FRET systems. Considering the generality of the cyclic peptide-based polymeric nanotubes as supramolecular scaffolds, we believe that this approach provides a powerful supramolecular strategy to fabricate fluorescent materials with tuneable luminescence as well as stimuli-responsive properties.

Conflicts of interest

There are no conflicts to declare.

Acknowledgements

The National Natural Science Foundation of China (22101124; Q. S.) and the European Research Council (TUSUPO 647106; Q. S., S. P.) are acknowledged for financial support. The authors thank the University of Warwick Polymer Characterisation Research Technology Platform for size exclusion chromatography facilities. We also acknowledge Dr Robert Dalgliesh (ISIS, Oxford, U.K.), Ms. Maria Kariuki (University of Warwick), and Ms. Sophie Hill (University of Warwick) for the assistance with the SANS experiment, and Ms. Sofia Goia (University of Warwick) and Prof. Vasilios Stavros (University of Warwick) for the help with time-resolved fluorescence spectroscopy measurement. We thank the STFC for the allocation of the beam time at ISIS (RB1920524).

References

1 W. R. Algar, M. Massey, K. Rees, R. Higgins, K. D. Krause, G. H. Darwish, W. J. Peveler, Z. Xiao, H.-Y. Tsai, R. Gupta, K. Lix, M. V. Tran and H. Kim, *Chem. Rev.*, 2021, **121**, 9243–9358.
2 L. Zhu, X. Li, Q. Zhang, X. Ma, M. Li, H. Zhang, Z. Luo, H. Ågren and Y. Zhao, *J. Am. Chem. Soc.*, 2013, **135**, 5175–5182.
3 G. Lukinavičius, L. Reymond, K. Umezawa, O. Sallin, E. D'Este, F. Göttfert, H. Ta, S. W. Hell, Y. Urano and K. Johnsson, *J. Am. Chem. Soc.*, 2016, **138**, 9365–9368.

4 Q. Qi, C. Li, X. Liu, S. Jiang, Z. Xu, R. Lee, M. Zhu, B. Xu and W. Tian, *J. Am. Chem. Soc.*, 2017, **139**, 16036–16039.
5 H. Wu, Y. Chen and Y. Liu, *Adv. Mater.*, 2017, **29**, 1605271.
6 L. Gu, H. Shi, L. Bian, M. Gu, K. Ling, X. Wang, H. Ma, S. Cai, W. Ning, L. Fu, H. Wang, S. Wang, Y. Gao, W. Yao, F. Huo, Y. Tao, Z. An, X. Liu and W. Huang, *Nat. Photonics*, 2019, **13**, 406–411.
7 A. Vollrath, S. Schubert and U. S. Schubert, *J. Mater. Chem. B*, 2013, **1**, 1994–2007.
8 K. Li and B. Liu, *Chem. Soc. Rev.*, 2014, **43**, 6570–6597.
9 L. D. Lavis and R. T. Raines, *ACS Chem. Biol.*, 2014, **9**, 855–866.
10 E. Kim, Y. Lee, S. Lee and S. B. Park, *Acc. Chem. Res.*, 2015, **48**, 538–547.
11 X.-H. Jin, C. Chen, C.-X. Ren, L.-X. Cai and J. Zhang, *Chem. Commun.*, 2014, **50**, 15878–15881.
12 Y. Li, T. Liu, H. Liu, M.-Z. Tian and Y. Li, *Acc. Chem. Res.*, 2014, **47**, 1186–1198.
13 C. Wang, W. Chi, Q. Qiao, D. Tan, Z. Xu and X. Liu, *Chem. Soc. Rev.*, 2021, **50**, 12656–12678.
14 S. Sasaki, G. P. C. Drummen and G.-I. Konishi, *J. Mater. Chem. C*, 2016, **4**, 2731–2743.
15 L. Yuan, W. Lin, K. Zheng and S. Zhu, *Acc. Chem. Res.*, 2013, **46**, 1462–1473.
16 V. S. Padalkar and S. Seki, *Chem. Soc. Rev.*, 2016, **45**, 169–202.
17 J. Zhang, B. He, Y. Hu, P. Alam, H. Zhang, J. W. Y. Lam and B. Z. Tang, *Adv. Mater.*, 2021, **33**, 2008071.
18 J. Mei, N. L. C. Leung, R. T. K. Kwok, J. W. Y. Lam and B. Z. Tang, *Chem. Rev.*, 2015, **115**, 11718–11940.
19 Z. Zhang, G. Sun, W. Chen, J. Su and H. Tian, *Chem. Sci.*, 2020, **11**, 7525–7537.
20 S. Qiu, Z. Zhang, Y. Wu, F. Tong, K. Chen, G. Li, L. Zhang, Z. Wang, D.-H. Qu and H. Tian, *CCS Chem.*, 2021, **3**, 2239–2248.
21 J.-M. Lehn, *Angew. Chem., Int. Ed. Engl.*, 1990, **29**, 1304–1319.
22 B. Qin, Z. Yin, X. Tang, S. Zhang, Y. Wu, J.-F. Xu and X. Zhang, *Prog. Polym. Sci.*, 2020, **100**, 101167.
23 K. Liu, Y. Kang, Z. Wang and X. Zhang, *Adv. Mater.*, 2013, **25**, 5530–5548.
24 D. B. Amabilino, D. K. Smith and J. W. Steed, *Chem. Soc. Rev.*, 2017, **46**, 2404–2420.
25 Z. Huang and X. Ma, *Cell Rep. Phys. Sci.*, 2020, **1**, 100167.
26 J. Zhang, X. Zhao, H. Shen, J. W. Lam, H. Zhang and B. Z. Tang, *Adv. Photonics*, 2021, **4**, 014001.
27 H. Wu, Y. Chen, X. Dai, P. Li, J. F. Stoddart and Y. Liu, *J. Am. Chem. Soc.*, 2019, **141**, 6583–6591.
28 X.-L. Ni, S. Chen, Y. Yang and Z. Tao, *J. Am. Chem. Soc.*, 2016, **138**, 6177–6183.
29 Y. Ma, F. Yu, S. Zhang, P. She, S. Liu, W. Huang and Q. Zhao, *CCS Chem.*, 2020, **2**, 2437–2444.
30 J. Wang, N. Wang, G. Wu, S. Wang and X. Li, *Angew. Chem., Int. Ed.*, 2019, **58**, 3082–3086.
31 J. Wang, R. Yan, Y. Hu, G. Du, G. Liao, H. Yang, Y. Luo, X. Zheng, Y. Chen, S. Wang and X. Li, *Angew. Chem., Int. Ed.*, 2022, **61**, e202112290.
32 B. Li, T. He, X. Shen, D. Tang and S. Yin, *Polym. Chem.*, 2019, **10**, 796–818.
33 H. Nie, Z. Wei, X.-L. Ni and Y. Liu, *Chem. Rev.*, 2022, **122**, 9032–9077.
34 A. Liang, S. Dong, X. Zhu, F. Huang and Y. Cao, *Polym. Chem.*, 2015, **6**, 6202–6207.
35 K. E. Sapsford, L. Berti and I. L. Medintz, *Angew. Chem., Int. Ed.*, 2006, **45**, 4562–4589.
36 H.-Q. Peng, L.-Y. Niu, Y.-Z. Chen, L.-Z. Wu, C.-H. Tung and Q.-Z. Yang, *Chem. Rev.*, 2015, **115**, 7502–7542.
37 A. J. P. Teunissen, C. Pérez-Medina, A. Meijerink and W. J. M. Mulder, *Chem. Soc. Rev.*, 2018, **47**, 7027–7044.
38 L. Wu, C. Huang, B. P. Emery, A. C. Sedgwick, S. D. Bull, X.-P. He, H. Tian, J. Yoon, J. L. Sessler and T. D. James, *Chem. Soc. Rev.*, 2020, **49**, 5110–5139.
39 P.-P. Jia, L. Xu, Y.-X. Hu, W.-J. Li, X.-Q. Wang, Q.-H. Ling, X. Shi, G.-Q. Yin, X. Li, H. Sun, Y. Jiang and H.-B. Yang, *J. Am. Chem. Soc.*, 2021, **143**, 399–408.
40 S. Farazi, F. Chen, H. Foster, R. Boquiren, S. R. McAlpine and R. Chapman, *Polym. Chem.*, 2020, **11**, 425–432.
41 G. Wu, Z. Huang and O. A. Scherman, *Angew. Chem., Int. Ed.*, 2020, **59**, 15963–15967.
42 Q. Song, Z. Cheng, M. Kariuki, S. C. L. Hall, S. K. Hill, J. Y. Rho and S. Perrier, *Chem. Rev.*, 2021, **121**, 13936–13995.
43 R. J. Brea, C. Reiriz and J. R. Granja, *Chem. Soc. Rev.*, 2010, **39**, 1448–1456.
44 J. Y. Rho and S. Perrier, *ACS Macro Lett.*, 2021, **10**, 258–271.
45 R. Chapman, K. A. Jolliffe and S. Perrier, *Polym. Chem.*, 2011, **2**, 1956–1963.
46 E. Folgado, Q. Song, S. Perrier, V. Ladmiral and M. Semsarilar, *Polym. Chem.*, 2021, **12**, 4235–4243.
47 R. J. Brea, C. Reiriz and J. R. Granja, *Chem. Soc. Rev.*, 2010, **39**, 1448–1456.
48 S. C. Larnaudie, J. C. Brendel, I. Romero-Canelón, C. Sanchez-Cano, S. Catrouillet, J. Sanchis, J. P. C. Coverdale, J.-I. Song, A. Habtemariam, P. J. Sadler, K. A. Jolliffe and S. Perrier, *Biomacromolecules*, 2018, **19**, 239–247.
49 Q. Song, A. Kerr, J. Yang, S. C. L. Hall and S. Perrier, *Chem. Sci.*, 2021, **12**, 9096–9103.
50 J. Yang, X. Yu, J.-I. Song, Q. Song, S. C. L. Hall, G. Yu and S. Perrier, *Angew. Chem., Int. Ed.*, 2022, **61**, e202115208.
51 J. M. Priegue, I. Louzao, I. Gallego, J. Montenegro and J. R. Granja, *Org. Chem. Front.*, 2022, **9**, 1226–1233.
52 M. Cuerva, R. García-Fandiño, C. Vázquez-Vázquez, M. A. López-Quintela, J. Montenegro and J. R. Granja, *ACS Nano*, 2015, **9**, 10834–10843.
53 Q. Song, S. Goia, J. Yang, S. C. L. Hall, M. Staniforth, V. G. Stavros and S. Perrier, *J. Am. Chem. Soc.*, 2021, **143**, 382–389.
54 X. Zhang, S. Rehm, M. M. Safont-Sempere and F. Würthner, *Nat. Chem.*, 2009, **1**, 623–629.
55 H. Liu, Z. Hu, H. Zhang, Q. Li, K. Lou and X. Ji, *Angew. Chem., Int. Ed.*, 2022, **61**, e2022035.